ACS OMEGA

Open Access

http://pubs.acs.org/journal/acsodf

Article

Piperazine-Based Co(III), Ni(II), Cu(II), and Zn(II) Carbodithioate Complexes as Potential Anticancer Agent

Seema Gupta, Alok Shukla, Shivendra Kumar Pandey, Shalini Jha, Berhanu Zewde, Arbind Acharya, Raymond John Butcher, and M. K. Bharty*

Cite This: *ACS Omega* 2025, 10, 13829−13838

Read Online

ACCESS | Metrics & More | Article Recommendations | Supporting Information

ABSTRACT: The development of facile and cost-effective anticancer metallodrugs possessing minimal side effects is urgently needed. Piperazine-containing anticancer drugs are already available on the market. A piperazine-based potassium 4-(ethoxycarbonyl)piperazine-1-carbodithioate [pecpcdt] (**L**) ligand and its metal complexes $[Co(ecpcdt)_3]$ (**1**), $[Ni(ecpcdt)_2]$ (**2**), $[Cu(ecpcdt)_2]$ (**3**), and $[Zn(ecpcdt)_2]$ (**4**) were synthesized. These compounds were characterized by different spectroscopic methods and single-crystal X-ray crystallography data. Ni(II) and Cu(II) complexes have distorted square planar geometry, whereas the Co(III) complex has distorted octahedral geometry around the metal ions. Complexes are weakly fluorescent in the solution compared to the free ligand. The complexes were further examined for their *in vitro* anticancer activities against the primary Dalton's lymphoma (DL) cells along with standard drug cisplatin. The anticancer studies of metal complexes have been performed through various biochemical assays, and the findings thus obtained suggest that they demonstrate an effective anticancer activity. $[Co(ecpcdt)_3]$ (**1**) shows superior cytotoxicity against DL cells than complexes $[Cu(ecpcdt)_2]$ (**3**), $[Zn(ecpcdt)_2]$ (**4**), and cisplatin. The superiority preferences of these complexes follows $[Co(ecpcdt)_3]$ (**1**) > [pecpcdt] > $[Cu(ecpcdt)_2]$ (**3**) > $[Ni(ecpcdt)_2]$ (**2**) > $[Zn(ecpcdt)_2]$ (**4**). Further assays were performed on a cobalt(III) complex having the highest efficacy to gain insights into the mechanism of cell death and showed that reduced mitochondrial membrane potential and increased mitochondrial ROS production, highlighting mitochondrial-dependent apoptosis as the major mechanism for tumor cell death. On the other hand, the viability of normal splenocytes was minimally affected by the $[Co(ecpcdt)_3]$ (**1**) treatment.

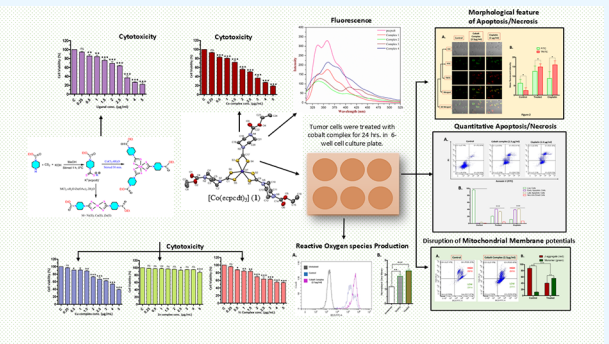

INTRODUCTION

Cancer remains one of the most serious health concerns of modern times, exerting a large impact on individuals, families, and societies worldwide. According to estimates from the World Health Organization (WHO) based on data from more than 100 nations, cancer is either the first or second largest cause of death before the age of 70. Recently, it has been estimated that there are over 10.0 million cancer-related fatalities worldwide and 19.3 million newly diagnosed cases of cancer. One of the major challenges facing contemporary global research concerning cancer is finding a cure.[1] There are several cancer therapies available, but chemotherapy is the most often used due to its higher survival rate than that of the others. Several metal complexes, such as oxaliplatin and cisplatin, are being used to treat various cancer cell types but come with a lot of drawbacks. The use of cisplatin and its derivative led to serious side effects such as nephrotoxicity, ototoxicity, and gastrointestinal toxicity.[2] Acute adverse effects on the body being treated and a limited therapeutic window have led to the use of nonplatinum-based metal ions, such as ruthenium, gold, iridium, rhenium, etc., which have displayed promising results in recent years.[3−5]

The first-row transition metal complexes have received attention due to their high abundance, intrinsic toxicity, and potential interference with endogenous metal ion pathways than late transition metals.[6] The first-row transition metal complexes are also appealing since the homeostasis and signaling of endogenous metal ions play a significant role in both healthy and disease states, and their alteration or disruption may open translational opportunities to take advantage of weaknesses in illness.[7] As essential trace elements, iron, cobalt, nickel, copper, and zinc can be employed as structural and catalytic cofactors that are involved in a variety of biological processes.[8] Cobalt, a cofactor for vitamin B_{12},

Received: July 30, 2024
Revised: March 1, 2025
Accepted: March 11, 2025
Published: April 1, 2025

Scheme 1. Synthesis of [pecpcdt] and Its Co(III), Ni(II), Cu(II), and Zn(II) Complexes

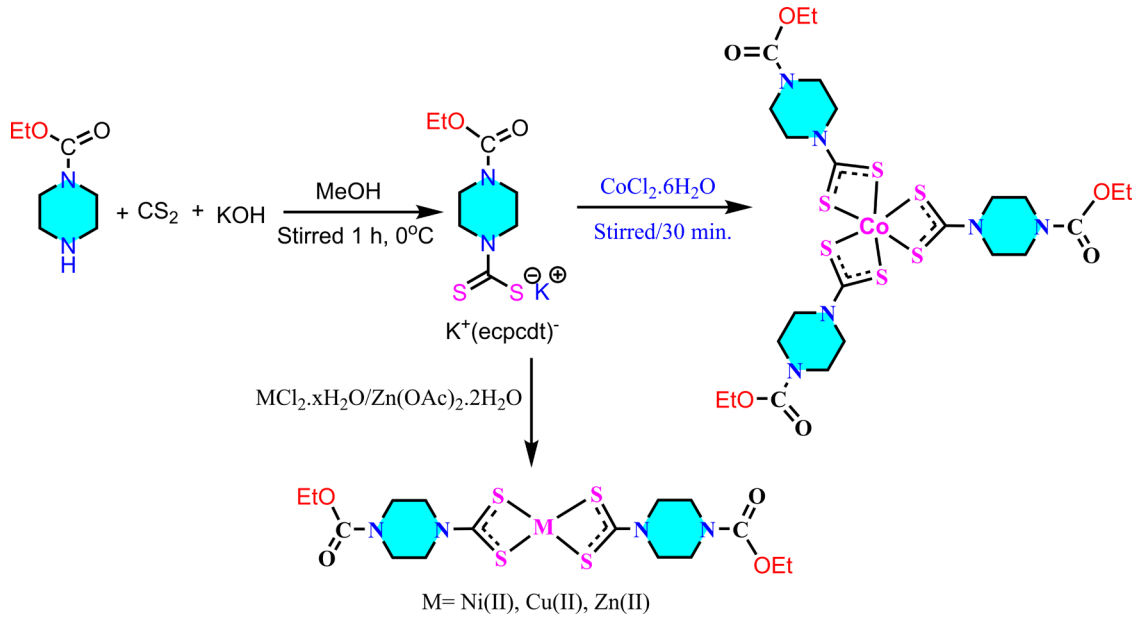

possesses the ability to control DNA synthesis and retain optimal nervous system and neurological functions.[9,10] Methyl-S-coenzyme M-reductase, hydrogenase, urease, and few various other enzymes all include nickel, which is essential for the transport of RNA and DNA.[11] Copper is less damaging to humans than nonessential metals like platinum.[12] More than 3000 proteins and enzymes contain zinc, which participates in immune system function, DNA synthesis, and protein synthesis.[13,14] As Zn(II) is a strong Lewis acid that is redox inactive, it can support an array of coordination geometries and has a tendency toward rapid ligand exchange. As a result, Zn(II) complexes are likely to function substantially more than traditional platinum medicines.[15]

The anticancer potential of metallodrugs can be tuned effectively with a suitable choice of ligand. The piperazine moiety is widely encountered in biologically active compounds used in various therapeutic applications, such as anticancer,[16] antibacterial,[17] and antifungal,[18] which has been acknowledged as a preferred structure in drug discovery. Some anticancer drugs are already available in the market containing piperazine moieties such as Palbociclib and Ribociclib (for treatment of metastatic breast cancer), Avapritinib (treatment of gastrointestinal stromal tumor), Trilaciclib (for mitigation of chemotherapy-induced myelosuppression in small cell lung cancer), Entrectinib (for treatment of metastatic nonsmall cell lung cancer), etc.[19] The Carbodithioates (CDTs) are given to patients at prescribed intervals to minimize the toxicity of platinum-based medications.[20] It is also known that platinum(II) complexes of CDTs have notable anticancer capabilities; in certain instances, their cytotoxic efficacy outperformed that of cisplatin.[21,22] Several CDT-containing metal complexes have been reported for anticancer activity.[23,24] In particular, Li et al. have reported platinum(II) complexes with methyl hydrazinecarbodithioate derivatives of indolin-2-one and found them to be efficient anticancer agents HCT-116, MCF-7, and MDA-MB-231 cell lines.[25] Amir et al. have reported the platinum(II) complexes based on 4-(4-methoxyphenyl)piperazine-1-carbodithioate as efficient anticancer agents.[26] Nawaz et al. have reported *N,N′*-dibenzyl-1-carbodithioate- and 4-(2-hydroxyethyl)piperazine-1-carbodithioate-based Pd(II) complexes and found that complexes have potent anticancer activity against HepG2 cells than standard drug doxorubicin.[24] Recently, Jaiswal et al. have prepared potassium azepane-1-carbodithioate (acdt) ligand and its metal complexes [Co(acdt)$_3$], [Cu(acdt)$_2$], [Zn$_2$(μ_2-acdt)$_2$(acdt)$_2$], and [PhHg(acdt)] and found them to be efficient against MDA-MB-231 cancer cells. They also found that the Co(III) complex increases the nitric oxide level more efficiently than other metal complexes in MDA-MB-231 cells.[27] Beebe et al. have prepared mixed ligand Co(III) complex with 9-anthraldehyde-N(4)-methylthiosemicarbazone and 1,10-phenanthroline. One of the Co(III) complexes they prepared has shown potency against 4T1-luc metastatic mammary breast cancer cells with IC$_{50}$ = 34.4 μM.[28] Dithiocarbazate-based complexes of Fe(III), Co(III), Ni(II), and Zn(II) have been synthesized and evaluated for their efficacy as antineoplastic agents against various cancer cells. Among them, the Co(III) complex exhibited higher anticancer efficacy than other complexes and cisplatin against MCF-7 and A549 cancer cells.[29] Dutta et al. have reported photoactive Co(III) complexes with a mixed ligand of the N,N-donor α-diimine ligands with naturally occurring flavonoids chrysin and silibinin. The complexes exhibited notable cytotoxicity against cervical (HeLa) and lung (A549) cancer cells when exposed to visible light (400−700 nm), resulting in low micromolar IC$_{50}$ values (2.3−3.4 μM) and a phototoxicity index of about 15−30. In addition, the complexes exhibited remarkably minimal toxicity toward normal lung epithelial cells.[30] Recently, Co(III) polypyridine containing sulfasalazine as a coligand is reported as a ferroptosis inducer. The complex exhibited the ability to eliminate both individual cancer cells and multicellular tumor spheroids of colon carcinoma.[31]

Thus, piperazine-appended CDTs ligand and its complexes have not been explored as anticancer agents against Dalton's lymphoma cells. Also, the spectral, structural, and mechanisms of anticancer action of these complexes have not been studied in detail. Also, the anticancer potential of different metal centers with the same ligand has not been explored much.

https://doi.org/10.1021/acsomega.4c06972
ACS Omega 2025, 10, 13829−13838

Keeping these facts, we have synthesized piperazine-appended CDTs ligand potassium 4-(ethoxycarbonyl) piperazine-1-carbodithioate [pecpcdt] and its complexes [Co(ecpcdt)$_3$] (**1**), [Ni(ecpcdt)$_2$] (**2**), [Cu(ecpcdt)$_2$] (**3**), and [Zn(ecpcdt)$_2$] (**4**). These complexes are fully characterized with different spectroscopic techniques, viz., UV−vis, IR, and single-crystal X-ray data for Co (III), Ni (II), and Cu (II) complexes. Further, the antiproliferative activity of these complexes was assessed against Dalton's Lymphoma cells (DL) along with *cisplatin* employing various biochemical assays.

EXPERIMENTAL SECTION

Materials and Methods. The details regarding chemicals used, crystallography, and anticancer studies have been given in the Supporting Information.

Synthesis of [pecpcdt]. To a solution of ethyl piperazine-1-carboxylate (1 mmol, 0.146 mL), carbon disulfide (1 mmol, 0.06 mL) and ethanolic solution of potassium hydroxide (1 mmol, 0.056 g) was added dropwise with continuous stirring, and the reaction is first stirred for 1 h on an ice bath. After the completion of the reaction, a white precipitate of potassium 4-(ethoxycarbonyl)piperazine-1-carbodithioate [pecpcdt] obtained was filtered off, washed with ethanol, and air-dried (Scheme 1).

Yield: 87%; M.P.: 268 °C. Anal. found: C, 35.05; H, 4.35; N, 10.60; S, 23.05%. Anal. Calcd for $C_8H_{13}KN_2O_2S_2$ (272.43): C, 35.27; H, 4.81; N, 10.28; S, 23.54. IR (KBr, cm^{-1}): 3009, 2982, 2906, 2863 ν(C−H$_{piperazine}$), 1693 ν(C═O), 1456 ν(C−H$_{bending}$), 1406 ν(C−N), 1210 ν(C−O), 1031 ν(C═S). ^{1}H NMR (500 MHz, D_2O, δ, ppm) 4.39 (t, J = 5.0 Hz, 4H), 4.20 (q, J= 10 Hz, 2H), 3.60 (t, J= 5 Hz, 4H), 1.30 (t, J = 7.4 Hz, 3H). ^{13}C NMR (126 MHz, D_2O, δ, ppm) 209.58 (>C−S), 157.35 (>C−N), 62.79, 50.56 (piperazine ring), 42.97 (CH_2), 13.92 (CH_3). UV−vis ($\lambda_{max,}$ DMF) 300 nm.

Preparation of Metal Complexes. A methanolic solution of $CoCl_2{\cdot}6H_2O$ (0.079 g, 0.33 mmol), $NiCl_2{\cdot}6H_2O$ (0.11 g, 0.5 mmol), $CuCl_2{\cdot}2H_2O$ (0.085 g, 0.5 mmol), and $Zn(OAc)_2{\cdot}2H_2O$ (0.11 g, 0.5 mmol) in an equimolar ratio [L:M = 2:1, 3:1 for cobalt(III) complex] were added separately into four separate stirring solution of freshly prepared solution of [pecpcdt] (**L**) to yielded complexes [Co(ecpcdt)$_3$] (**1**), [Ni(ecpcdt)$_2$] (**2**), [Cu(ecpcdt)$_2$] (**3**), and [Zn(ecpcdt)$_2$] (**4**), respectively, and the mixture was again stirred for 30 min at room temperature. After the completion of the reaction, colored precipitates of the [Co(ecpcdt)$_3$] (**1**) (blackish green), [Ni(ecpcdt)$_2$] (**2**) (pastel green), [Cu(ecpcdt)$_2$] (**3**) (green), and [Zn(ecpcdt)$_2$] (**4**) (white) obtained were filtered off, washed with methanol, and air-dried. Single crystals of these complexes suitable for X-ray analysis were grown by slow evaporation of the above solution over 10−30 days (Scheme 1).

*Synthesis of [Co(ecpcdt)$_3$] (**1**).* Yield: 65%; M.P.: 183 °C, Anal. found: C, 37.14; H, 4.95; N, 11.60; S, 25.05%. Anal. Calcd for $C_{24}H_{39}N_6CoO_6S_6$ (758.90): C, 37.94; H, 5.13; N, 11.06; S, 25.29. IR (KBr, cm^{-1}): 2922, 2857 ν(C−H$_{piperazine}$), 1701 ν(C═O), 1421 ν(C−N), 978 ν(C═S), 767, 536 ν(Co−S). ^{1}H NMR (500 MHz, $CDCl_3$, δ, ppm) 4.17 (q, J = 6.9 Hz, 6H, −CH_3), 3.88 (q, J = 6.4 Hz, 12H), 3.57 (d, J = 6.8 Hz, 12H), 1.2 (t, J = 7.2 Hz, 9H). The ^{13}C NMR (126 MHz $CDCl_3$, δ, ppm): 205.63 (>C−S), 155.32 (−C-N), 62.05, 45.07 (piperazine ring), 42.84 (CH_2), 14.69 (CH_3). UV−vis ($\lambda_{max,}$ DMF) at 325 and 650 nm.

*Synthesis of [Ni(ecpcdt)$_2$] (**2**).* Yield: 63%; M.P.: 294 °C, Anal. found: C, 36.05; H, 4.30; N, 10.40; S, 24.05%. Anal. Calcd for $C_{16}H_{26}N_4NiO_4S_4$ (525.34): C, 36.54; H, 4.94; N, 10.65; S, 24.36. IR (KBr, cm^{-1}): 2981, 2910, 2861 ν(C−H$_{piperazine}$), 1704 ν(C═O), 1504, 1427 ν(C−N), 983 ν(C═S), 547, 480 ν(Ni−S). ^{1}H NMR (500 MHz, $CDCl_3$, δ, ppm) 4.09 (q, J = 5.0 Hz, 4H, CH_2), 3.71−3.74 (q, J = 6.4 Hz, 8H, CH_2), 3.32−48 (d, J = 6.8 Hz, 8H, CH_2), 1.20 (t, J = 5.0 Hz, 6H, CH_3). The ^{13}C NMR (126 MHz $CDCl_3$, δ, ppm): 203.57 (>C−S), 154.40 (−C-N), 61.18, 45.07 (piperazine ring), 42.84 (CH_2), 14.51 (CH_3). UV−vis ($\lambda_{max,}$ DMF) 273, 430, and 610 nm.

*Synthesis of [Cu(ecpcdt)$_2$] (**3**).* Yield: 62%; M.P.: 238 °C, Anal. found: C, 35.90; H, 4.30; N, 10.35; S, 24.45%. Anal. Calcd for $C_{16}H_{26}N_4CuO_4S_4$ (530.19): C, 36.21; H, 4.90; N, 10.56; S, 24.14. IR (KBr, cm^{-1}): 2984, 2916, 2862 ν(C−H$_{piperazine}$), 1714 ν(C═O), 1423 ν(C−N), 979 ν(C═S), 772, and 540 ν(Cu−S). UV−vis ($\lambda_{max,}$ DMF) spectra: 272, 431, and 632 nm.

*Synthesis of [Zn(ecpcdt)$_2$] (**4**).* Yield: 66%; M.P.: 263 °C, Anal. found: C, 36.45; H, 4.40; N, 10.35; S, 24.40%. Anal. Calcd for $C_{16}H_{26}N_4ZnO_4S_4$ (532.03): C, 36.08; H, 4.88; N, 10.52; S, 24.05. IR (KBr, cm^{-1}): 2992, 2922, 2857 ν(C−H$_{piperazine}$), 1704 ν(C═O), 1432 ν(C−N), 1008 ν(C═S), 541, 475 ν(Zn−S). ^{1}H NMR (600 MHz, DMSO-d_6) δ 4.03−4.08 (m, 12H, piperazine ring + CH_2 of ethyl), 3.46−3.48 (t, J = 5.2 Hz, 8H, other CH_2 protons of piperazine), 1.19 (t, J = 7.1 Hz, 6H, CH_3). The ^{13}C NMR (151 MHz DMSO-d_6, δ, ppm): 204.70 (>C−S), 154.61 (−C-N), 61.51, 50.77 (piperazine ring), 43.14 (CH_2), 14.58 (CH_3). UV−vis ($\lambda_{max,}$ DMF): 277, 340 nm.

RESULTS AND DISCUSSION

Potassium 4-(ethoxycarbonyl)piperazine-1-carbodithioate [pecpcdt] was prepared by a reaction of ethyl piperazine-1-carboxylate, carbon disulfide, and potassium hydroxide in an ethanolic solution. The targeted metal complexes were obtained by the reaction of the ligand with the corresponding metal salts in an appropriate ratio. After the successful characterization of metal complexes, we examined the antiproliferative activity on Dalton's lymphoma cells.

IR Spectra. The IR spectrum of [pecpcdt] showed the characteristic bands of CH, C═O, C−N, C−S, and stretching vibrations. The C−H$_{piperazine}$ stretching vibrations were observed in the range of 3009−2982 cm^{-1}. The C═O stretching frequency was found at 1693 cm^{-1}, indicating the presence of a carbonyl group. In addition, the compound also showed CH (methyl and methylene groups) symmetrical and asymmetrical stretching vibrations at 2906 and 2863 cm^{-1}, respectively. Further, C−N stretching vibrations were observed at 1406 cm^{-1}, respectively. The C−S stretching vibrations were observed at 1031 cm^{-1} (Figure S2). The IR spectra of complexes **1**−**4** showed characteristic bands of CH, C═O, C−N, C−S, and stretching vibrations. In complexes **1**−**4**, C−H$_{piperazine}$ stretching vibrations were observed in the range of 2922−2992 cm^{-1}, respectively. The C═O group stretching frequency was observed in the 1701−1714 cm^{-1} range in complexes **1**−**4**. In addition, all complexes also showed a CH$_{methyl}$ symmetrical vibration around 2857 cm^{-1}, whereas the asymmetrical vibration merged with C−H$_{piperazine}$ stretching vibrations (∼2950). Further, the C−N stretching vibration was observed in the range of 1421−1432 cm^{-1} for complexes **1**−**4**. A new band of M-S stretching vibrations range of 475−536

https://doi.org/10.1021/acsomega.4c06972
ACS Omega 2025, 10, 13829−13838

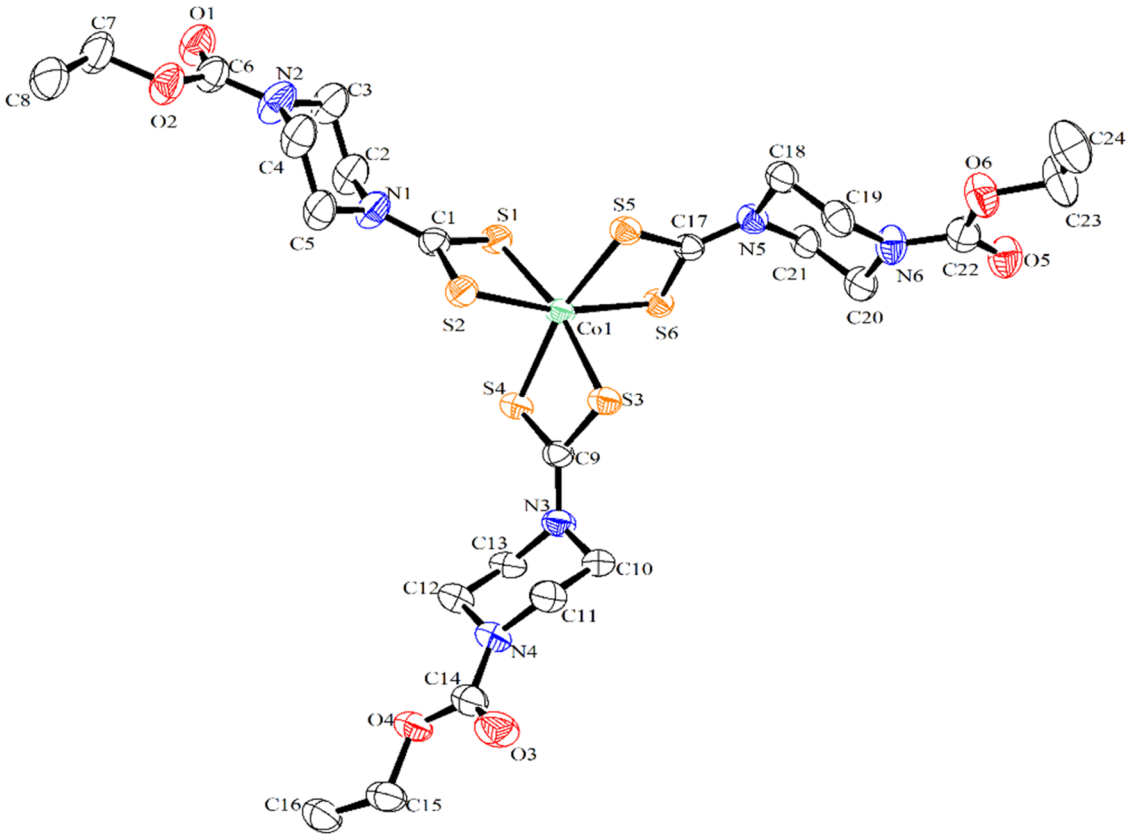

Figure 1. ORTEP Diagram of [Co(ecpcdt)$_3$] (**1**) at the 40% Probability Level. Hydrogen Atoms Are Omitted for Clarity.

cm^{-1}. The C−S stretching vibration was observed in the range of 978−1008 cm^{-1} in complexes 1−4 (Figures S3−S6). A negative shift of approximately 50 cm^{-1} in the ν(C═S) stretching frequency was observed in all complexes, indicating the formation of metal−sulfur bonds. A positive shift of approximately 10 cm^{-1} was observed in the ν(C−N) stretching frequency, further supporting the formation of complexation.[24−32]

Electronic Absorption Spectra and Magnetic Moments. The observed magnetic moment for the Cu(II) complex is approximately 1.72 μ_B, indicating the existence of a single unpaired electron. However, other complexes are diamagnetic, as indicated by their magnetic moment values, which are near 0.4 μ_B, and the recorded NMR spectra of these complexes. The electronic absorption spectra of [pecpcdt] and complexes **1**−**4** were recorded in a 50 μM DMF solution. The ligand [pecpcdt] and its complexes **1**−**4** exhibit prominent absorption bands at 300, 325, 273, 272, and 277 nm, respectively, which can be attributed to intraligand charge transfer (ILCT) transitions (Figure S7A). The complex **1** is diamagnetic, indicating the presence of Co(III) in a low-spin octahedral geometry. It shows a band at 650 nm, which is assigned to the $^1A_{1g} \rightarrow {}^1T_{1g}$ transition characteristic of Co(III) in octahedral coordination[33] (Figure S7B). Complex **2** reveals two additional peaks at 430 and 610 nm. These bands are attributed to d−d transitions (specifically, $^1A_{1g} \rightarrow {}^1B_{1g}$ and $^1A_{1g} \rightarrow {}^1B_{2g}$ transitions) within the metal d-orbitals. The diamagnetic behavior of complex **1**, along with the observed d−d transitions, supports the square planar geometry around the Ni(II) central metal ion.[34] Complex **3** shows two bands at 431 and 632 nm, attributed to d−d transitions ($d_{xy} \rightarrow d_{x^2-y^2}$ and $d_{z^2} \rightarrow d_{x^2-y^2}$ transition) in the metal d-orbitals. These transitions suggest a square planar geometry around the Cu(II) ion (Figure S7B). Since Zn(II) has a d^{10} electronic configuration, the electronic spectrum of complex **4** shows only absorption bands at 277 and 330 nm. These bands are attributed to $\pi \rightarrow \pi^*$ and ILCT (intraligand charge transfer) transitions (Figure S7A).[32,,36]

Emission Spectra. Emission spectra of the ligand [pecpcdt] and complexes **1**−**4** were obtained in a 50 μM DMF solution between 200 and 800 nm. Ligand [pecpcdt] shows an emission band at 358 nm upon excitation at 300 nm. However, complex **1** excited at 325 nm exhibits an emission maximum at 358 nm. Other complexes **2**, **3**, and **4** display emission maxima at 337, 342, and 378 nm upon excitation at 275 nm. Thus, the above results suggest that the ligand and complexes **1**−**4** are fluorescent (Figure S8).

^{1}H and ^{13}C NMR Spectra. The ^{1}H NMR spectrum of potassium 4-(ethoxycarbonyl)piperazine-1-carbodithioate [pecpcdt] exhibits two signals at δ 4.39 and 3.60 ppm due to the CH_2 protons of the piperazine ring. Due to ethyl protons, two signals were observed at δ 4.20 and 1.30 ppm. The ^{13}C NMR spectrum of [pecpcdt] showed two signals at δ 209.58 and 157.35 ppm due to the >C═S and >C−N carbons, respectively. The signals for CH_2 and CH_3 carbons were observed at δ 62.79 and 13.92 ppm, respectively. The piperazine ring carbons appear at 50.56 and 42.97 ppm. ^{1}H NMR spectra of complexes showed signals in the range δ 7.45−8.60 and 7.45−8.62 ppm for complexes **1**, **2**, and **4** are assigned to the protons of the piperazine ring of the ligand. Complexes **1**, **2**, and **4** showed N-CS_2 carbon signals at 205.63, 203.57, and 204.70 ppm, respectively, which signifies the delocalization of electrons and metal−sulfur bonding in the four-membered CS_2M chelate ring (Figures S9−S16).

https://doi.org/10.1021/acsomega.4c06972
ACS Omega 2025, 10, 13829−13838

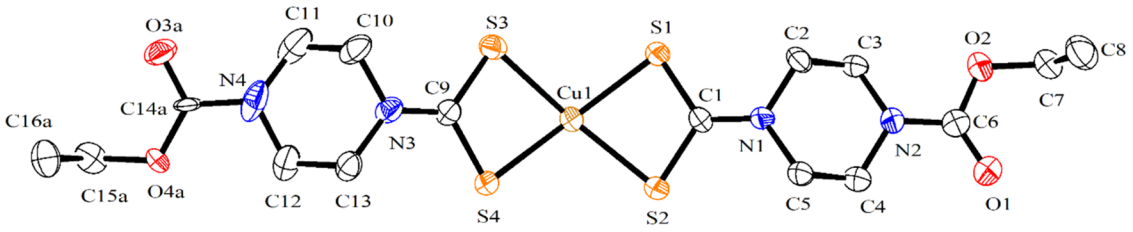

Figure 2. ORTEP diagram of [Cu(ecpcdt)$_2$] (**3**) at the 40% probability level. Only the main contributing part is shown. H atoms and other disordered parts are omitted.

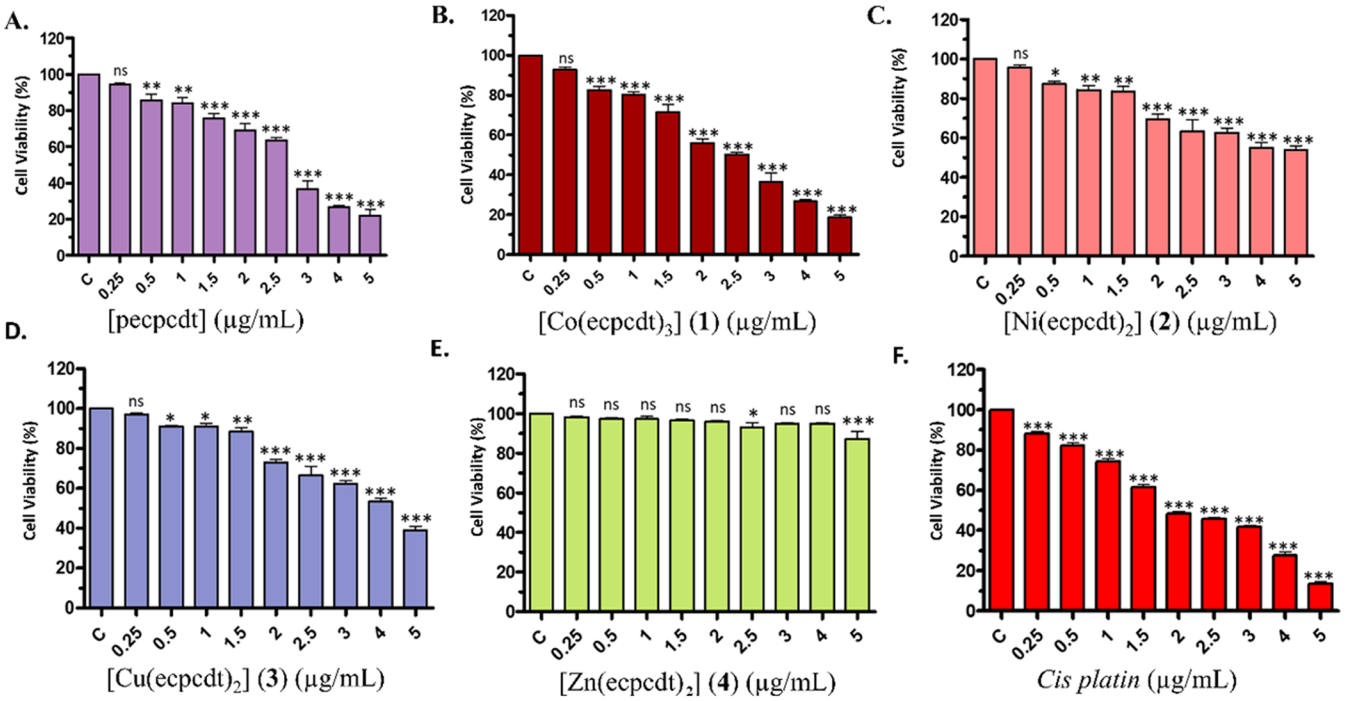

Figure 3. Cell viability was evaluated using the standard MTT assay detailed in the materials and methods. Tumor cells were subjected to 24 h treatments with varying concentrations of [pecpcdt] (**1**) (A), [Co(ecpcdt)$_3$] (**1**) (B), [Ni(ecpcdt)$_2$] (**2**) (C), [Cu(ecpcdt)$_2$] (**3**) (D), [Zn(ecpcdt)$_2$] (**4**) (E), and cisplatin (F). The cytotoxic effects were quantified, and the results are presented in a bar diagram, indicating the percentage of mean ± SD. Statistical analysis involved a one-way analysis of variance, followed by Bonferroni's multiple comparison post-test, across at least three independent experiments. Significance levels were denoted as $^{**}p < 0.01$ and $^{***}p < 0.001$.

Crystal Structure Description. The details of data collection, structure solution, and refinement are listed in Table S1. Selected bond lengths and angles for complexes are given in Tables S2 and S3. Further, the weak intermolecular interactions are listed in Tables S4−S6.

Crystal Structure Description of [Co(ecpcdt)$_3$] (1). The ORTEP diagram displaying [Co(ecpcdt)$_3$] (**1**) along with the atom numbering system is depicted in Figure 1. Complex **1** crystallizes in a triclinic system with the space group *P*-1. The coordination sphere of the cobalt center is accomplished by coordinating with six dithiocarbamato sulfur atoms originating from three units of the same ligand. This interaction results in the formation of CS_2Co chelates, each comprising four members. The Co−S bond lengths in complex **1** are Co1−S2 = 2.2713(16), Co1−S5 = 2.2763(15), Co1−S3 = 2.2775(17), Co1−S4 = 2.2786(15), Co1−S6 = 2.2855(15), and Co1−S1 = 2.2974(18) Å (Table S2). These bond lengths closely resemble those reported for analogous complexes.[32,37,38] The bite angles around Co(III) are found at 76.51(6)°, 77.57(6)°, and 76.21(5)°, demonstrating a significant deviation from the regular octahedral (Oh) geometry (Table S3). Within the Co(III) chelate ring, the carbon−sulfur bond distances are observed to be intermediate between single and double bond distances, and S−C bond distances are found to be in the range of 1.711−1.741 Å. These findings suggest significant charge delocalization within the chelate ring.[27,38] Further, the structure is stabilized by intra- and intermolecular C−H···S and C−H···O hydrogen bonding interactions as depicted in Figures S17 and S18, respectively, and bond distances for these interactions are given in Table S4. These interactions contribute to stabilizing the structure of the complex and play an essential role in constructing a supramolecular architecture.

Crystal Structure Description of [Ni(ecpcdt)$_2$] (2) and [Cu(ecpcdt)$_2$] (3). Complexes **2** and **3** are isostructural, and only one ORTEP diagram is given here (Figure 2). The crystallographic unit of complexes **2** and **3** contains two units of complexes, which closely interact with each other through ionic kind of weak M···S (M = Ni/Cu, 2.706 and 2.716 Å, respectively) interaction (Figures S19 and S20, respectively), which is like previous reports and considerably larger than the standard Ni/Cu−S bond (~2.3 Å).[27,39−41] In addition, one part of the ester moiety is disordered in complex **2** and split into two parts a and b with occupancies 0.51 and 0.49, and

https://doi.org/10.1021/acsomega.4c06972
ACS Omega 2025, 10, 13829−13838

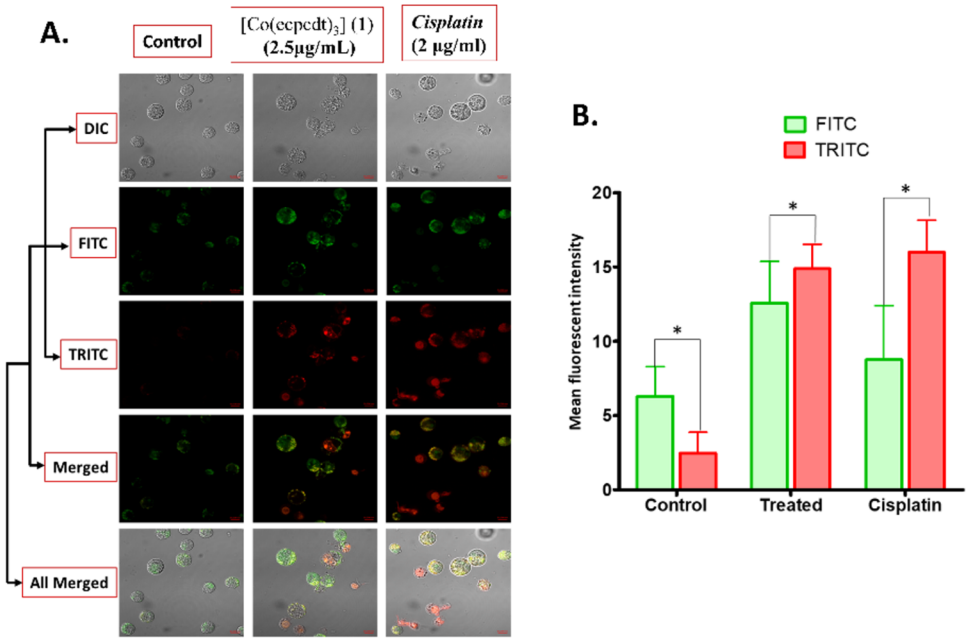

Figure 4. Morphological features of apoptosis, necrosis, and plasma membrane integrity were evaluated through AO/EB dual staining. (A) Images were captured using DIC, FITC, and TRITC channels on a confocal microscope (Zeiss LSM 780) at 60× magnification. (B) Mean fluorescent intensity of AO/EB in control, cobalt-complex-treated, and cisplatin-treated tumor cells is represented in a bar diagram. Statistically significant at $*p < 0.1$.

major contributing part a is taken for discussion (C(14)−O(3A) = 1.458(12)). Similar to complex **2**, complex **3** also has a distorted piperazine and ester moiety and is split into parts a and b with occupancies of 0.56 and 0.44, and the main contributing part a is taken for discussion (C(14)−O(3A) = 1.221(11)). The ORTEP plot of $[Cu(ecpcdt)_2]$ (**3**), along with the atom numbering scheme, is shown in Figure 2. In complexes $[Ni(ecpcdt)_2]$ (**2**) (Figure S1) and $[Cu(ecpcdt)_2]$ (**3**), the coordination environment of the metal center is formed by four dithiocarbamato sulfurs from two ligand units, resulting in a distorted square planar geometry around Ni(II) and Cu(II) metal ions. All of the metal−sulfur bond distances are about 2.1976(9) and 2.2090(9) Å (Table S4). The bond distances observed closely match those reported for previously studied copper(II) and Ni(II) dithiocarbamato complexes.[27,35,39−41] The comparable bite angles {S(1)−Ni−S(2) = 76.70(5)° and S(2)−Cu(1)−S(1) = 76.50(4)°} observed in the two metal chelates of complexes $[Ni(ecpcdt)_2]$ (**2**) and $[Cu(ecpcdt)_2]$ (**3**) are considerably lower than the ideal bond angle of 90°, suggesting a distorted square planar geometry at the metal center. The metal is placed slightly above the plane of four S atoms by 0.371 and 0.375 Å for complexes **2** and **3**, respectively. Notably, the four S atoms are not perfectly coplanar, and the distortion from planarity is due to the weak interaction of one of the sulfur atoms with the metal atom of the adjacent molecule. There are three distinct types of N−C bond lengths present in complexes **2** and **3**. The C1−N1 (1.322(11) and 1.324(5) Å) bond lengths are the shortest, followed by the N2−C6 (1.355(11) and 1.357(6) Å) bond lengths and the N−C bonds in the six-membered ring, which are the longest (N1−C2 1.477(11) and 1.463(5) Å) for complexes **2** and **3**. In complexes **2** and **3**, the structures are stabilized by intra- and intermolecular C−H···S and C−H···O hydrogen bonding interactions as depicted in Figures S21−S28, and bond distances for these interactions are given in Tables S5 and S6.

Antitumor Studies. *Metal Complexes Reduced Tumor Cells' Viability.* The MTT assay evaluated the cytotoxic and antiproliferative effects of the ligand and all of the complexes on tumor cells. The ligand exhibited the highest cell death at 5.0 μg/mL of concentration (Figure 3A). However, complex $[Zn(ecpcdt)_2]$ (**4**) was the least effective, inducing only 5.62% cell death at its highest concentration of 5 μg/mL (Figure 3E). The complex $[Ni(ecpcdt)_2]$ (**2**) was more effective than $[Zn(ecpcdt)_2]$ (**4**), causing 48% cell death at 5 μg/mL (Figure 3C). The complex $[Cu(ecpcdt)_2]$ (**3**) demonstrated a notable decrease in cell viability with an IC_{50} of 3.82 μg/mL (Figure 3B). The complex $[Co(ecpcdt)_3]$ (**1**) emerged as the most potent among all, with activity comparable to the standard drug cisplatin (Figure 3F). Its cytotoxic potential was dose-dependent, achieving the highest cell death at 5 μg/mL, with an IC_{50} value of 2.5 μg/mL (Figure 3B). These observations are consistent with previous reports.[27,42] Due to the superior cytotoxicity demonstrated by the cobalt complex, subsequent experiments utilized treatment with its IC_{50} concentration (2.5 μg/mL), and the outcomes were compared with the IC_{50} (2.0 μg/mL) of the standard drug cisplatin. Further, the viability of normal splenocytes was minimally affected by the $[Co(ecpcdt)_3]$ (**1**) treatment, as demonstrated in Figure S29. However, there are only a few reports available on the antiproliferative effects of synthetic complexes against DL cells. Under comparable conditions (24 h of incubation), the antiproliferative activity of the synthesized $[Co(ecpcdt)_3]$ (**1**) on DL cells is compared with the previously described compounds. The synthesized complex has anticancer activity that is much better than earlier findings (Table S7).

Induction of Apoptosis and Necrosis in Tumor Cells. Programmed cell death is crucial for the anticancer efficacy of drugs. Hence, we assessed the ability of $[Co(ecpcdt)_3]$ (**1**), comparing it with that of cisplatin, to induce apoptosis in tumor cells through microscopy and flow cytometry. Morphological changes were examined using AO/EB staining,

https://doi.org/10.1021/acsomega.4c06972
ACS Omega 2025, 10, 13829−13838

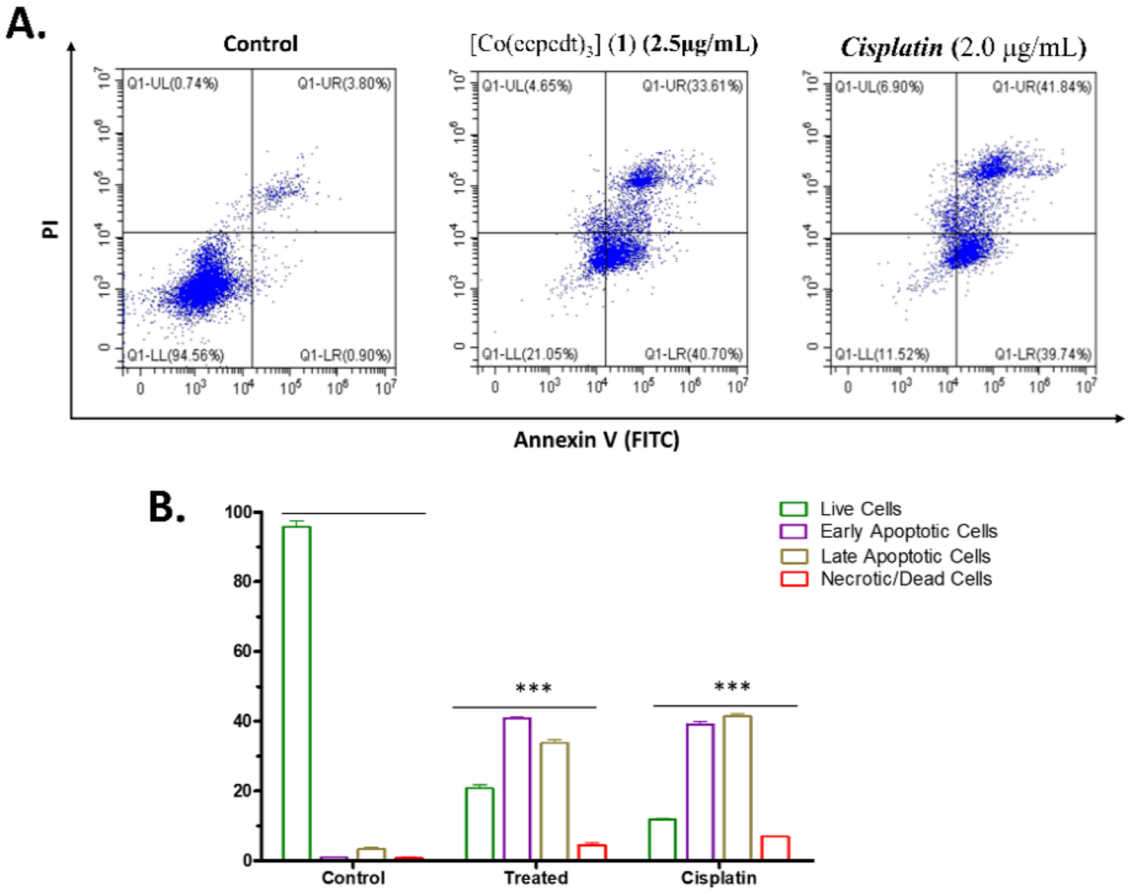

Figure 5. Tumor cells were treated with specified concentrations of the cobalt complex and the standard anticancer drug cisplatin separately for 24 h. A quantitative assessment of apoptosis induced by the cobalt complex was conducted using Annexin-V/PI staining followed by flow cytometry. (A) Flow cytometry dot plot illustrating the counts of live, early apoptotic, late apoptotic, and necrotic cells in control, $[Co(ecpcdt)_3]$ (**1**)-treated and cisplatin-treated groups. (B) Bar diagram depicting the percentage of apoptotic tumor cells in all three groups, with statistical significance measured at $^{***}p < 0.001$.

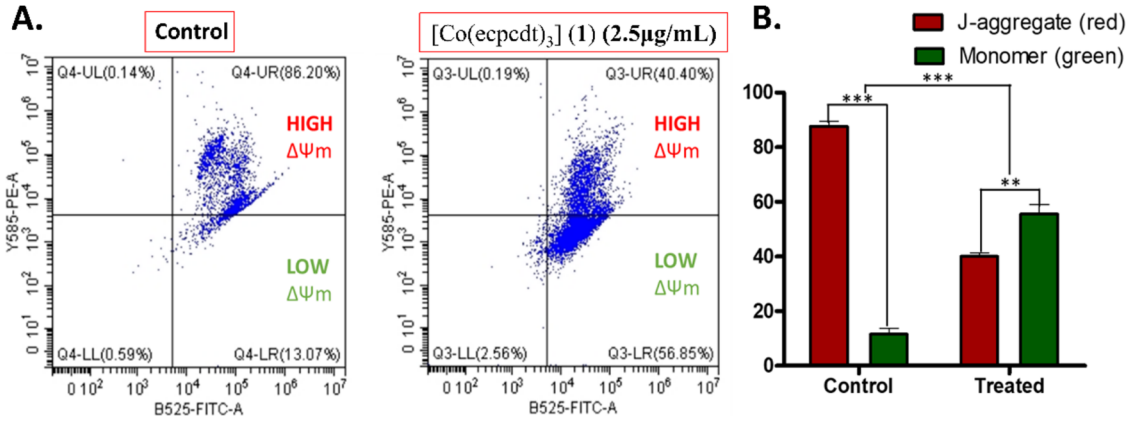

Figure 6. Flow cytometry analysis of mitochondrial membrane potential using the JC-1 assay in tumor cells treated with the cobalt complex. (A) FACS quadrant illustrating a shift in the cell percentage toward green fluorescence, indicating reduced mitochondrial potential. (B) Bar diagram depicting the percentage of tumor cells emitting red fluorescence (JC-1's J aggregates) and green fluorescence (JC-1 monomer). Statistical significance was measured at $^{**}p < 0.01$, $^{***}p < 0.001$.

revealing significant apoptosis and necrosis caused by cobalt complex treatment (Figure 4A). Cells in early apoptosis displayed a brilliant green and yellowish nucleus, while those in late apoptosis emitted orange fluorescence. Necrotic and dead cells exhibited a dense orange and red nucleus.[43] As shown in Figure 4B, the mean fluorescent intensities of AO/EB have increased, signifying enhanced permeabilization of the dye within apoptotic and necrotic cells. This suggests a loss of plasma membrane integrity in cells treated with the cobalt complex and cisplatin. For a more precise and quantitative evaluation of apoptotic cells, Annexin-V/PI staining, followed by flow cytometry, was performed. Annexin-V binds to phosphatidylserine on apoptotic cell surfaces, and PI, a membrane-impermeable dye, enters cells with compromised

https://doi.org/10.1021/acsomega.4c06972
ACS Omega 2025, 10, 13829−13838

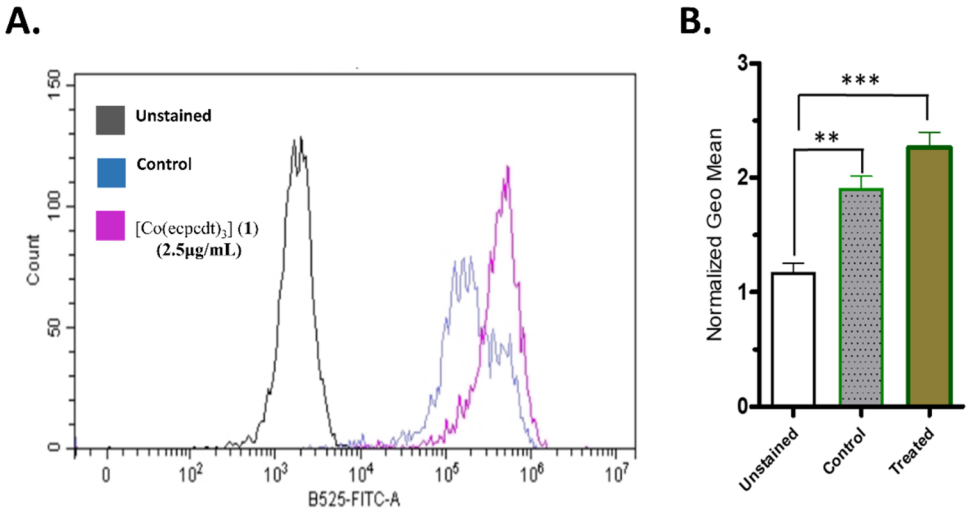

Figure 7. Impact of cobalt complex treatment on ROS production in tumor cells was evaluated by using the H_2DCFDA assay. ROS levels were analyzed via flow cytometry using the FL-1 channel. (A) Flow cytometry histogram displays increased ROS production, evident from the right shift in overlaid histograms. (B) Bar diagram illustrates the enhancement in the geomean during flow cytometry. Statistically significant at $^{**}p < 0.01$, $^{***}p < 0.001$.

membranes.[33] Treatment with the cobalt complex at its IC_{50} concentration for 24 h led to a striking increase in early apoptotic cells from 0.90 to 40.70%, and late apoptotic cells rose from 3.80 to 33.61% compared to control ($p < 0.001$). The apoptotic effects induced by the [Co(ecpcdt)$_3$] (**1**) were nearly comparable to those caused by the standard anticancer drug cisplatin (Figure 5A,B).

Disruption of ΔΨm in Tumor Cells. A JC-1 assay was performed to identify whether apoptosis initiated in tumor cells by [Co(ecpcdt)$_3$] (**1**) treatment was dependent on or independent of mitochondria. Flow cytometry data indicated a significant shift in the cell population, with 56.85% displaying a decreased mitochondrial membrane potential upon cobalt complex treatment (Figure 6A). JC-1 dye's potential-dependent accumulation in mitochondria was evident, with a shift from green to red fluorescence at 590 nm, indicative of higher ΔΨm. Conversely, monomeric JC-1 exhibited green fluorescence at 529 nm, corresponding to lower ΔΨm.[34] The observed disruption in mitochondrial membrane potential, as evidenced by the change in the percentage of cells fluorescing red to green, suggests a mitochondrial-dependent mechanism underlying apoptosis (Figure 6B).

Enhanced ROS Production in Tumor Cells. The induction of apoptosis through mitochondria is closely associated with elevated ROS generation within cells.[44] We assessed the oxidative stress of [Co(ecpcdt)$_3$] (**1**)-treated tumor cells by detecting the level of ROS generation. ROS levels in tumor cells were measured using the nonfluorescent, cell-permeable dye H_2DCFDA, which, when exposed to ROS, was converted to the fluorescent 2′,7′-dichlorofluorescein. Flow cytometry analysis of H_2DCFDA-stained cells demonstrated an increase in the level of ROS production upon treatment with the cobalt complex. This was evident from a right-shifted histogram, indicative of elevated ROS levels in [Co(ecpcdt)$_3$] (**1**)-treated tumor cells (Figure 7A). Moreover, the higher fold change in the geometric mean, obtained through flow cytometry analysis control and [Co(ecpcdt)$_3$] (**1**)-treated tumor cells in comparison, was depicted in a bar diagram (Figure 7B).

CONCLUSIONS

A new ligand potassium-1-ethoxycarbonyl-piperazine-4-carbodithioate [pecpcdt] (**L**) and its complexes [Co(ecpcdt)$_3$] (**1**), [Ni(ecpcdt)$_2$] (**2**), [Cu(ecpcdt)$_2$] (**3**), and [Zn(ecpcdt)$_2$] (**4**) have been synthesized and characterized by various spectroscopic techniques. The molecular structures of **1**, **2**, and **3** were confirmed by single-crystal X-ray crystallography. In the presence of the carbodithioate ligand, complex **1** is formed by the conversion of Co(II) to Co(III) by aerial oxidation, forming a six-coordinate distorted octahedral Tris-carbodithioate Co(III) complex. The crystal structures of complexes **1**, **2**, and **3** are stabilized by various types of intermolecular and intramolecular hydrogen bondings. Further, the evaluation of the anticancer potential of the ligand and these complexes against Dalton's lymphoma cells has been performed. Among the four complexes and the ligand tested, the cobalt complex was found as the most potent in inducing cytotoxic and antiproliferative effects. The cobalt complex displayed remarkable cytotoxic activity against tumor cells of non-Hodgkin's lymphoma cells, comparable to that of cisplatin. The apoptosis and necrosis caused by the cobalt complex concurrently decline ΔΨm and increase intracellular ROS production and oxidative stress. In addition, the viability of normal splenocytes is marginally affected by the cobalt complex. The anticancer potential of the cobalt complex observed in this study makes it a promising anticancer agent for further exploration.

ASSOCIATED CONTENT

Data Availability Statement

The data underlying this study are available in the published article and its Supporting Information.

Supporting Information

The Supporting Information is available free of charge at https://pubs.acs.org/doi/10.1021/acsomega.4c06972.

IR, NMR, UV−vis, and X-ray data interaction figures. (PDF)

https://doi.org/10.1021/acsomega.4c06972
ACS Omega 2025, 10, 13829−13838

Accession Codes

Supplementary crystallographic data for compounds can be obtained through CCDC 2300088, 2300089, and 2300087 contain the supplementary crystallographic data for complexes **1**, **2**, and **3**. These data can be obtained free of charge via http://www.ccdc.cam.ac.uk/conts/ retrieving.html, or from the Cambridge Crystallographic Data Centre, 12 Union Road, Cambridge CB2 1EZ, UK; fax: (+44) 1223-336- 033; or e-mail: deposit@ccdc.cam.ac.uk.

AUTHOR INFORMATION

Corresponding Author

M. K. Bharty − *Department of Chemistry, Banaras Hindu University, Varanasi 221005, India;* orcid.org/0000-0002-6116-2439; Email: mkbharty@bhu.ac.in

Authors

Seema Gupta − *Department of Chemistry, Banaras Hindu University, Varanasi 221005, India;* orcid.org/0000-0002-7933-3128

Alok Shukla − *Department of Zoology, Banaras Hindu University, Varanasi 221005, India*

Shivendra Kumar Pandey − *Department of Chemistry, Banaras Hindu University, Varanasi 221005, India*

Shalini Jha − *Department of Chemistry, Banaras Hindu University, Varanasi 221005, India*

Berhanu Zewde − *Department of Chemistry, Howard University, Washington, District of Columbia 20059, United States*

Arbind Acharya − *Department of Zoology, Banaras Hindu University, Varanasi 221005, India*

Raymond John Butcher − *Department of Chemistry, Howard University, Washington, District of Columbia 20059, United States*

Complete contact information is available at: https://pubs.acs.org/10.1021/acsomega.4c06972

Author Contributions

In manuscript preparation, all authors have given their input and approval for submission. S.G.: conceptualization, methodology, data curation, formal analysis, visualization, and writing the original draft. A.S.: data curation, software, investigation, formal analysis, writing the original draft, validation. S.K.P.: methodology, writing the original draft, formal analysis, and validation. S.J.: data curation and writing, reviewing, and editing of the manuscript. B.Z.: data curation. A.A.: supervision, resources, validation, and writing, reviewing, and editing of the manuscript. R.J.B.: data curation, software, methodology, and validation. M.K.B.: supervision, resources, methodology, investigation, formal analysis, validation, writing, reviewing, and editing of the manuscript, project administration, and funding acquisition.

Notes

The authors declare no competing financial interest.

ACKNOWLEDGMENTS

M. K. Bharty gratefully acknowledges Banaras Hindu University, Varanasi, for IoE Dev. Scheme No.6031 for financial assistance. We also thank Howard University and the National Science Foundation Major Research Instrumentation program (NSF DMR-2117502) for financially supporting the acquisition of the Rigaku Synergy-S single-crystal X-ray diffractometer used in this study.

REFERENCES

(1) Chanu, M. T.; Asem, S. S. Cancer Disease and Its' Understanding from the Ancient Knowledge to the Modern Concept. *World J. Adv. Res. Rev.* **2022**, *15* (2), 169−176.

(2) Oun, R.; Moussa, Y. E.; Wheate, N. J. The Side Effects of Platinum-Based Chemotherapy Drugs: A Review for Chemists. *Dalton Trans.* **2018**, *47* (19), 6645−6653.

(3) Aggarwal, S. K. A Histochemical Approach to the Mechanism of Action of Cisplatin and Its Analogues. *J. Histochem. Cytochem.* **1993**, *41* (7), 1053−1073.

(4) Brozovic, A.; Ambriović-Ristov, A.; Osmak, M. The Relationship between Cisplatin-Induced Reactive Oxygen Species, Glutathione, and BCL-2 and Resistance to Cisplatin. *Crit. Rev. Toxicol.* **2010**, *40* (4), 347−359.

(5) Chaurasia, R.; Pandey, S. K.; Singh, D. K.; Bharty, M. K.; Ganesan, V.; Hira, S. K.; Manna, P. P.; Bharti, A.; Butcher, R. J. Antiproliferative Activity and Electrochemical Oxygen Evolution by Ni(II) Complexes of *N* ′-(Aroyl)-Hydrazine Carbodithioates. *Dalton Trans.* **2021**, *50* (40), 14362−14373.

(6) Barnham, K. J.; Bush, I. A. Biological metals and metal-targeting compounds in major neurodegenerative diseases. *Chem. Soc. Rev.* **2014**, *43* (19), 6727−6749.

(7) Zoroddu, M. A.; Aaseth, J.; Crisponi, G.; Medici, S.; Peana, M.; Nurchi, V. M. The Essential Metals for Humans: A Brief Overview. *J. Inorg. Biochem.* **2019**, *195*, 120−129.

(8) Heffern, M. C.; Yamamoto, N.; Holbrook, R. J.; Eckermann, A. L.; Meade, T. J. Cobalt Derivatives as Promising Therapeutic Agents. *Curr. Opin. Chem. Biol.* **2013**, *17* (2), 189−196.

(9) Deng, J.; Li, T.; Su, G.; Qin, Q.-P.; Liu, Y.; Gou, Y. Co(III) Complexes Based on α-N-Heterocyclic Thiosemicarbazone Ligands: DNA Binding, DNA Cleavage, and Topoisomerase I/II Inhibitory Activity Studies. *J. Mol. Struct.* **2018**, *1167*, 33−43.

(10) Munteanu, C. R.; Suntharalingam, K. Advances in Cobalt Complexes as Anticancer Agents. *Dalton Trans.* **2015**, *44* (31), 13796−13808.

(11) Masaryk, L.; Tesarova, B.; Choquesillo-Lazarte, D.; Milosavljevic, V.; Heger, Z.; Kopel, P. Structural and Biological Characterization of Anticancer Nickel(II) Bis(Benzimidazole) Complex. *J. Inorg. Biochem.* **2021**, *217*, No. 111395.

(12) Santini, C.; Pellei, M.; Gandin, V.; Porchia, M.; Tisato, F.; Marzano, C. Advances in copper complexes as anticancer agents. *Chem. Rev.* **2014**, *114* (1), 815−862.

(13) Kolenko, V.; Teper, E.; Kutikov, A.; Uzzo, R. Zinc and Zinc Transporters in Prostate Carcinogenesis. *Nat. Rev. Urol.* **2013**, *10* (4), 219−226.

(14) Haase, H.; Rink, L. Multiple Impacts of Zinc on Immune Function. *Metallomics* **2014**, *6* (7), 1175.

(15) Porchia, M.; Pellei, M.; Del Bello, F.; Santini, C. Zinc Complexes with Nitrogen Donor Ligands as Anticancer Agents. *Molecules* **2020**, *25* (24), 5814.

(16) Chen, F.-h.; Zhang, L.; Qiang, L.; Yang, Z.; Wu, T.; Zou, M.; Tao, L.; You, Q.; Li, Z.; Yang, Y.; Guo, Q.-L. Reactive Oxygen Species-Mitochondria Pathway Involved in LYG-202-Induced Apoptosis in Human Hepatocellular Carcinoma HepG2 Cells. *Cancer Lett.* **2010**, *296* (1), 96−105.

(17) Foley, T. L.; Rai, G.; Yasgar, A.; Daniel, T.; Baker, H. L.; Attene-Ramos, M.; Kosa, N. M.; Leister, W.; Burkart, M. D.; Jadhav, A.; Simeonov, A.; Maloney, D. J. 4-(3-Chloro-5-(Trifluoromethyl)-Pyridin-2-Yl)- *N* -(4-Methoxypyridin-2-Yl)Piperazine-1-Carbothioamide (ML267), a Potent Inhibitor of Bacterial Phosphopantetheinyl Transferase That Attenuates Secondary Metabolism and Thwarts Bacterial Growth. *J. Med. Chem.* **2014**, *57* (3), 1063−1078.

(18) Ji, Q.; Deng, Q.; Li, B.; Li, B.; Shen, Y. Design, Synthesis and Biological Evaluation of Novel 5-(Piperazin-1-Yl)Quinolin-2(1H)-One Derivatives as Potential Chitin Synthase Inhibitors and Antifungal Agents. *Eur. J. Med. Chem.* **2019**, *180*, 204−212.

(19) Romanelli, M. N.; Braconi, L.; Gabellini, A.; Manetti, D.; Marotta, G.; Teodori, E. Synthetic Approaches to Piperazine-Containing Drugs Approved by FDA in the Period of 2011−2023. *Molecules* **2024**, *29* (1), 68.
(20) Lemma, K.; Elmroth, S. K. C.; Elding, L. I. Substitution Reactions of [Pt(Dien)Cl]+, [Pt(Dien)(GSMe)]2+, Cis-$[PtCl_2(NH_3)_2]$ and Cis-$[Pt(NH_3)_2(GSMe)_2]^{2+}$ (GSMe = S-Methylglutathione) with Some Sulfur-Bonding Chemoprotective Agents. *J. Chem. Soc., Dalton Trans.* **2002**, *7*, 1281.
(21) Faraglia, G. Platinum(II) and Palladium(II) Complexes with Dithiocarbamates and Amines: Synthesis, Characterization and Cell Assay. *J. Inorg. Biochem.* **2001**, *83* (1), 31−40.
(22) Marzano, C.; Fregona, D.; Baccichetti, F.; Trevisan, A.; Giovagnini, L.; Bordin, F. Cytotoxicity and DNA Damage Induced by a New Platinum(II) Complex with Pyridine and Dithiocarbamate. *Chem.−Biol. Interact.* **2002**, *140* (3), 215−229.
(23) Fregona, D.; Giovagnini, L.; Ronconi, L.; Marzano, C.; Trevisan, A.; Sitran, S.; Biondi, B.; Bordin, F. Pt(II) and Pd(II) Derivatives of Ter-Butylsarcosinedithiocarbamate. *J. Inorg. Biochem.* **2003**, *93* (3−4), 181−189.
(24) Nawaz, H.; Waseem, A.; Zia-ur-Rehman; Nafees, M.; Arshad, M. N.; Rashid, U. Synthesis, Characterization, Cytotoxicity and Computational Studies of New Phosphine- and Carbodithioate-based Palladium (II) Complexes. *Appl. Organomet. Chem.* **2017**, *31* (11), No. e3771, DOI: 10.1002/aoc.3771.
(25) Li, Y.-S.; Peng, B.; Ma, L.; Cao, S.-L.; Bai, L.-L.; Yang, C.-R.; Wan, C.-Q.; Yan, H.-J.; Ding, P.-P.; Li, Z.-F.; Liao, J.; Meng, Y.-Y.; Wang, H.-L.; Li, J.; Xu, X. Synthesis, Crystal Structures and Antitumor Activity of Two Platinum(II) Complexes with Methyl Hydrazinecarbodithioate Derivatives of Indolin-2-One. *Eur. J. Med. Chem.* **2017**, *127*, 137−146.
(26) Amir, M. K.; Zia-ur-Rehman, Z.-R.; Hayat, F.; Khan, S. Z.; Hogarth, G.; Kondratyuk, T.; Pezzuto, J. M.; Tahir, M. N. Monofunctional Platinum (II) Dithiocarbamate Complexes: Synthesis, Characterization and Anticancer Activity. *RSC Adv.* **2016**, *6* (112), 110517−110524.
(27) Jaiswal, S.; Rai, N.; Chandra, S.; Verma, A.; Gautam, V.; Adhikari, M.; Singh, S.; Bharty, M. K. Design, synthesis, and structural evaluation of metal complexes of azepane-1-carbodithioate for targeting human breast cancer: investigating cytotoxic activity against the MDA-MB-231 cell line. *New J. Chem.* **2024**, *48* (30), 13589−13601.
(28) Beebe, S. J.; Celestine, M. J.; Bullock, J. L.; Sandhaus, S.; Arca, J. F.; Cropek, D. M.; Ludvig, T. A.; Foster, S. R.; Clark, J. S.; Beckford, F. A.; Tano, C. M.; et al. Synthesis, characterization, DNA binding, topoisomerase inhibition, and apoptosis induction studies of a novel cobalt (III) complex with a thiosemicarbazone ligand. *J. Inorg. Biochem.* **2020**, *203*, No. 110907.
(29) Gou, Y.; Jia, X.; Hou, L. X.; Deng, J. G.; Huang, G. J.; Jiang, H. W.; Yang, F. Dithiocarbazate−Fe (III), Co (III), Ni (II) and Zn (II) complexes: Design, synthesis, structure, and anticancer evaluation. *J. Med. Chem.* **2022**, *65* (9), 6677−6689.
(30) Dutta, J.; Bera, A.; Upadhyay, A.; Yadav, A. K.; Banerjee, S.; Sarkar, T.; Hussain, A. Photoactivated Anticancer Activity of Cobalt (III) Complexes with Naturally Occurring Flavonoids Chrysin and Silibinin. *ChemBioChem* **2024**, *25*, No. e202400484.
(31) Montesdeoca, N.; Johannknecht, L.; Efanova, E.; Heinen-Weiler, J.; Karges, J. Ferroptosis Inducing Co (III) Polypyridine Sulfasalazine Complex for Therapeutically Enhanced Anticancer Therapy. *Angew. Chem., Int. Ed.* **2024**, *63*, No. e202412585.
(32) Dulare, R.; Bharty, M. K.; Singh, A.; Singh, N. K. Synthesis, Spectral and Structural Studies of 1-Ethoxycarbonyl-Piperazine-4-Carbodithioate and Its Co(III), Zn(II) and Cd(II) Complexes. *Polyhedron* **2012**, *31* (1), 373−378.
(33) Bossy-Wetzel, E.; Green, D. R. Detection of Apoptosis by Annexin V Labeling. *Methods Enzymol.* **2000**, *322*, 15−18.
(34) Reers, M.; Smiley, S. T.; Mottola-Hartshorn, C.; Chen, A.; Lin, M.; Chen, L. B. Mitochondrial Membrane Potential Monitored by JC-1 Dye. *Methods Enzymol.* **1995**, *260*, 406−417.
(35) Singh, A.; Shiv, K.; Singh, R.; Bharty, M. K.; Manna, P. P.; Prasad, L. B. Antiproliferative Activity Ni(II), Cu(II), and Zn(II) Complexes of Dithiocarbamate: Synthesis, Structural Characterization, and Thermal Studies. *Dalton Trans.* **2024**, *53* (3), 1196−1208.
(36) Nath, P.; Bharty, M. K.; Maiti, B.; Bharti, A.; Butcher, R. J.; Wikaira, J. L.; Singh, N. K. Ag(I), Cu(II), Co(III) and Hg(II) Complexes and Metal-Assisted Products Derived from 4-Methyl-Piperidine-Carbodithioate: Syntheses, Structures, Thermal Analyses, Redox Behaviour and Fluorescence Properties. *RSC Adv.* **2016**, *6* (96), 93867−93880.
(37) Hogarth, G.; Rainford-Brent, E.-J.; Kabir, S. E.; Richards, I.; Wilton-Ely, J. D. E. T.; Zhang, Q. Functionalised Dithiocarbamate Complexes: Synthesis and Molecular Structures of 2-Diethylaminoethyl and 3-Dimethylaminopropyl Dithiocarbamate Complexes $[M\{S2CN(CH_2CH_2NEt_2)_2\}n]$ and $[M\{S2CN-(CH2CH2CH2NMe_2)_2\}n]$ (N = 2, M = Ni, Cu, Zn, Pd; N = 3, M = Co). *Inorg. Chim. Acta* **2009**, *362* (6), 2020−2026.
(38) Bharati, P.; Bharti, A.; Nath, P.; Bharty, M. K.; Butcher, R. J.; Singh, N. K. Synthesis, Spectral and Structural Characterization of Cobalt(III) Dithiocarbamato Complexes: Catalytic Application for the Solvent Free Enamination Reaction. *Polyhedron* **2015**, *102*, 375−385.
(39) Singh, A.; Kumar, R.; Shiv, K.; Pandey, S. K.; Bharty, M. K.; Butcher, R. J.; Prasad, L. B. Synthesis, Crystal Structure and Screening for Anticonvulsant and Antianxiety Activities of Three New Ni(II), Cu(II), and Zn(II) Dithiocarbamate Complexes. *J. Mol. Struct.* **2024**, *1298*, No. 137052.
(40) Jian, F.; Wang, Z.; Bai, Z.; You, X.; Fun, H. K.; Chinnakali, K.; Razak, I. A. The crystal structure, equilibrium and spectroscopic studies of bis (dialkyldithiocarbamate) copper (II) complexes [Cu2 (R2dtc) 4](dtc= dithiocarbamate). *Polyhedron* **1999**, *18* (26), 3401−3406.
(41) De Lima, G. M.; Menezes, D. C.; Cavalcanti, C. A.; Dos Santos, J. A.; Ferreira, I. P.; Paniago, E. B.; Wardell, J. L.; Wardell, S. M.; Krambrock, K.; Mendes, I. C.; Beraldo, H. Synthesis, characterisation and biological aspects of copper (II) dithiocarbamate complexes, $[Cu\{S2CNR(CH_2CH_2OH)\}_2]$, (R= Me, Et, Pr and CH_2CH_2OH). *J. Mol. Struct.* **2011**, *988* (1−3), 1−8.
(42) Singh, R. P.; Singh, A.; Prasad, L. B.; Shiv, K.; Hira, S. K.; Manna, P. P. Nickel (II), Copper (II), and Zinc (II) complexes of N-bis (4-methoxybenzyl) Dithiocarbamate: synthesis, characterization studies, and evaluation of antitumor activity. *J. Mol. Struct.* **2022**, *1264*, No. 133295.
(43) Russo, A.; Terrasi, M.; Agnese, V.; Santini, D.; Bazan, V. Apoptosis: A Relevant Tool for Anticancer Therapy. *Ann. Oncol.* **2006**, *17*, vii115−vii123.
(44) Matés, J. M.; Sánchez-Jiménez, F. M. Role of Reactive Oxygen Species in Apoptosis: Implications for Cancer Therapy. *Int. J. Biochem. Cell Biol.* **2000**, *32* (2), 157−170.

https://doi.org/10.1021/acsomega.4c06972
ACS Omega 2025, 10, 13829−13838